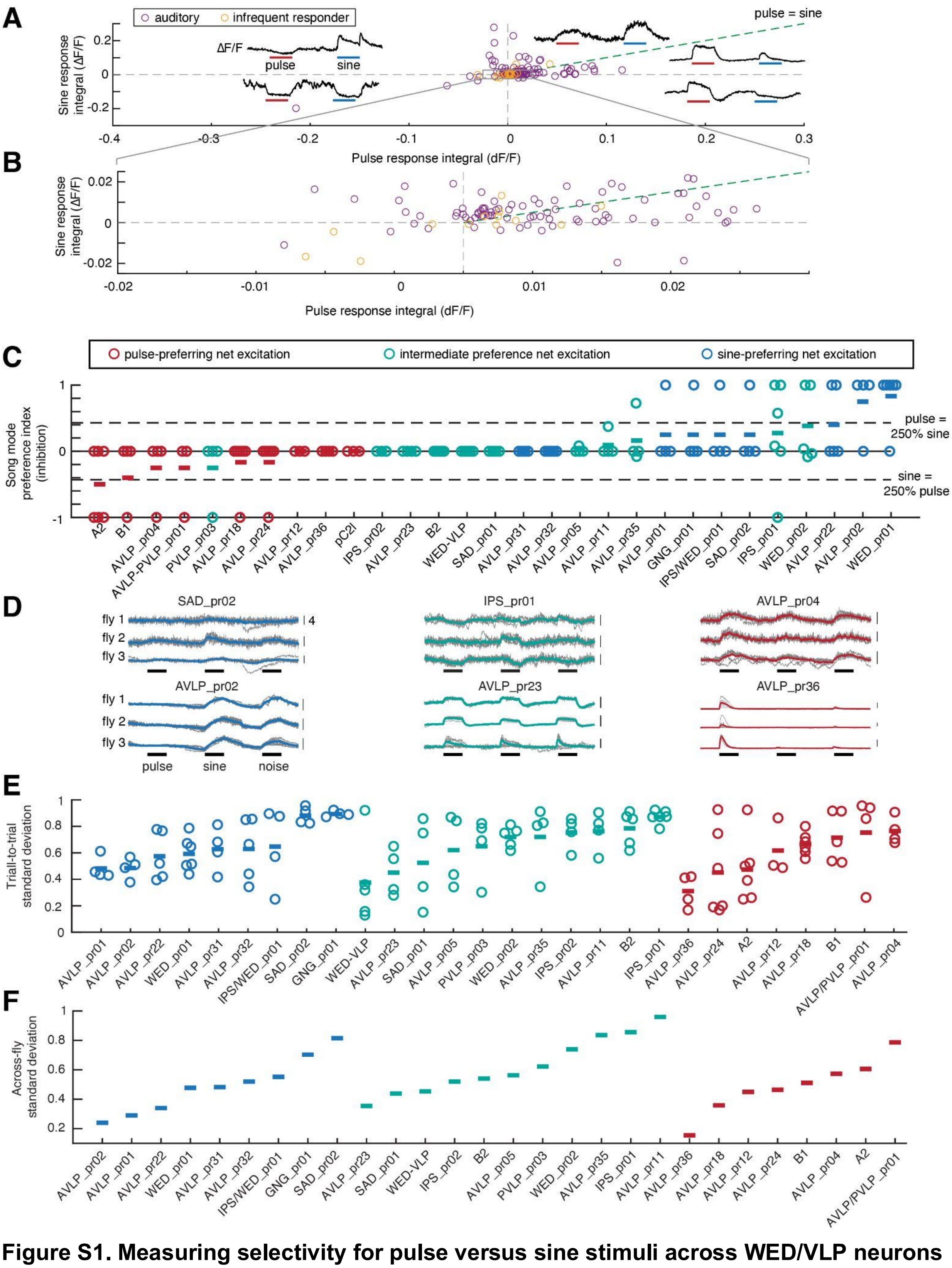

Figure S1. Measuring selectivity for pulse versus sine stimuli across WED/VLP neurons and response variability, related to Figure 3. A) The integral of each trial-averaged response (open circles) to pulse vs. the integral response to sine stimuli. Black box indicates region enlarged in (B). Each dot represents the responses from one fly. (C) Song mode preference index for net inhibition, which ranges from -1 for strongest inhibition to sine to +1 for strongest inhibition to pulse. Data are ordered along the x-axis according to the song mode preference index in Figure 3C. Each dot represents the responses from one fly, and horizontal lines indicate the D) Calcium responses to pulse, sine, and noise stimuli for 3 flies from 2 cell types from each song mode preference class. Z-scored responses to each trial are shown in grey, and the average within fly is shown in color. E) Trial-to-trial response variability for each cell type organized by song mode preference. F) Same as (E) for across-fly response variability. Each WED/VLP neuron type is colored according to its overall sine or pulse preference (see Figure 3).

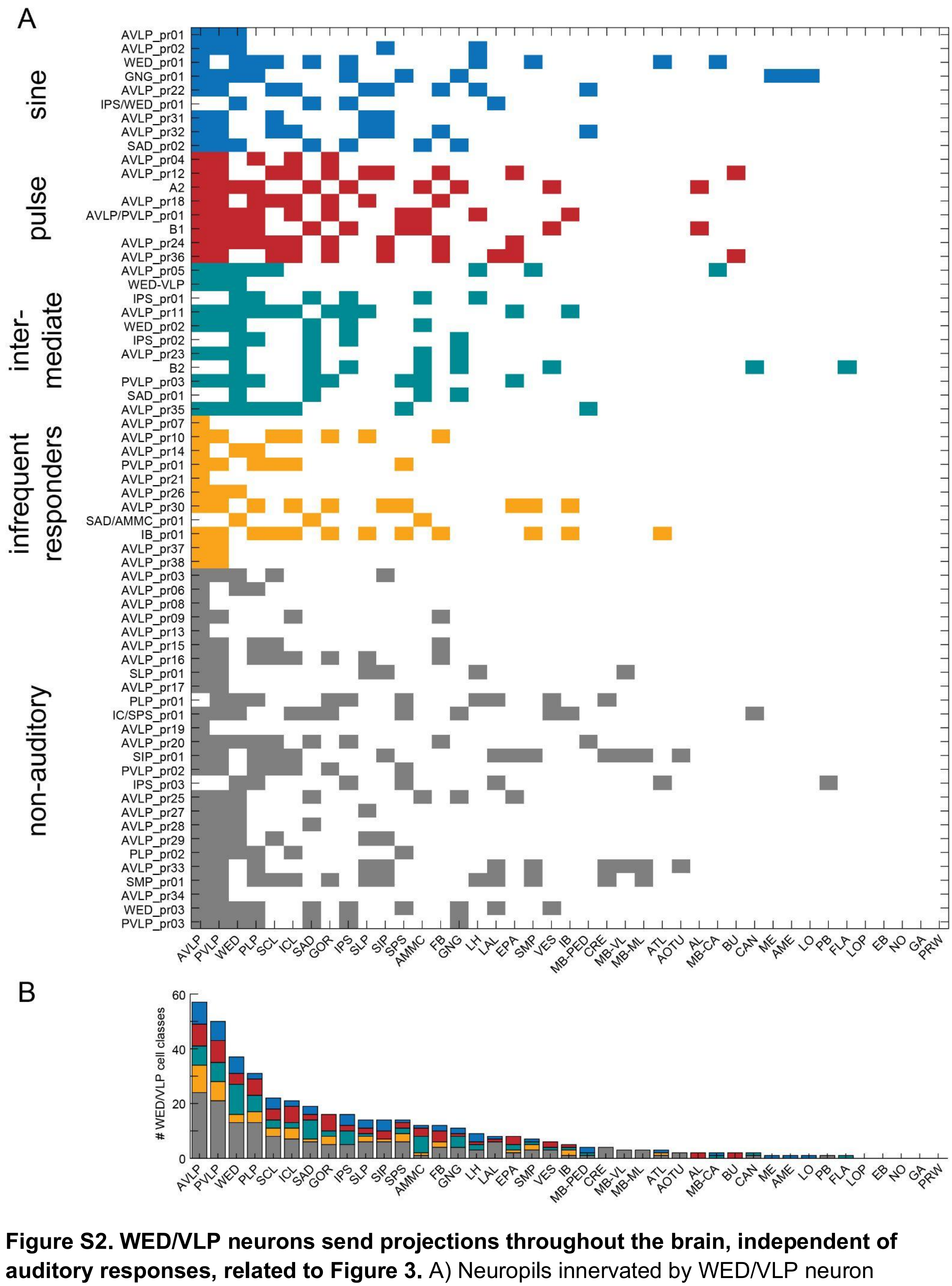

Figure S2. WED/VLP neurons send projections throughout the brain, independent of auditory responses, related to Figure 3. A) Neuropils innervated by WED/VLP neuron classes, defined as having at least 1% of a cell class's total volume in each neuropil. Each WED/VLP neuron type is colored according to its overall sine or pulse preference (see Figure 3). B) Histogram of the total number of WED/VLP cell classes with innervation in each neuropil. Neuropil abbreviations are listed in Table S1.

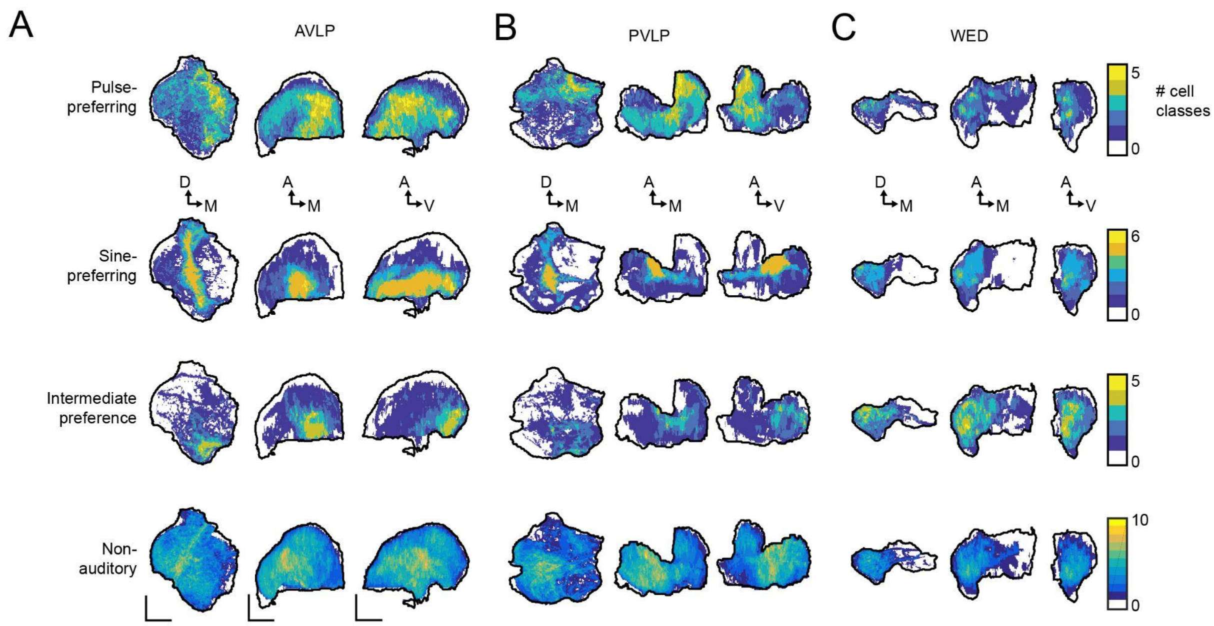

Figure S3. Auditory neurons are spatially segregated in the VLP according to song mode preference, related to Figure 2 and 3. A-C) 2D projections of the maximum number of WED/VLP cell classes with expression in voxels within the right hemisphere of the AVLP (A), PVLP (B), and WED (C) neuropils. In the AVLP, we found that pulse-preferring neurons most frequently targeted medial and anterior regions, whereas sine-preferring neurons were biased towards a posterior tract extending from ventral to dorsal areas. Neurons with intermediate preference targeted areas innervated by both pulse- and sine-preferring lines, whereas non-auditory lines most frequently targeted the lateral half of the AVLP. In the PVLP, projections of sine-preferring neurons were most common in an anterior region, roughly in the middle of the medial-lateral and dorsal-ventral axes, whereas projections of pulse-preferring neurons were found more medially and dorsally. In contrast to the AVLP, intermediate-preference lines innervated a region separate from the major areas innervated by pulse- and sine-preferring neurons. Non-auditory lines tended to innervate more lateral PVLP regions than auditory lines. In contrast to VLP projections, WED projections showed less pronounced differences between pulse- vs. sine-preferring, and auditory vs. non-auditory response categories. Taken together, these results suggest that sine and pulse preference largely arises in the VLP in separate anatomical regions, and that this transformation in stimulus preference likely occurs between WED projection and VLP projection neurons. Scale bars = 25 microns.

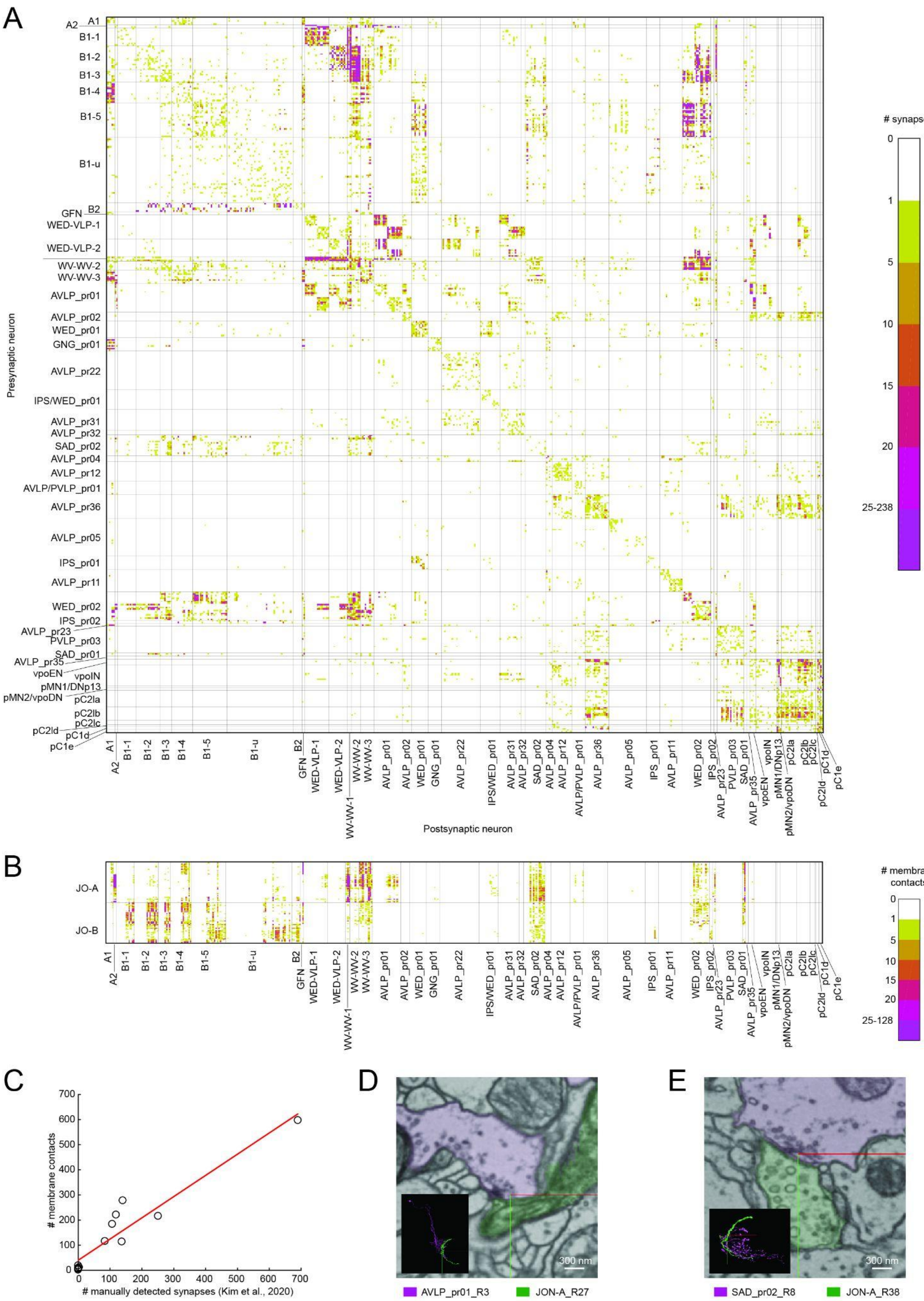

A
B
C
D
E
Presynaptic neuron
Postsynaptic neuron
synapses
0
1
5
10
15
20
25-238
A1
A2
B1-1
B1-2
B1-3
B1-4
B1-5
B1-u
GFN
B2
WED-VLP-1
WED-VLP-2
WV-WV-1
WV-WV-2
WV-WV-3
AVLP_pr01
AVLP_pr02
WED_pr01
GNG_pr01
AVLP_pr22
IPS/WED_pr01
AVLP_pr31
AVLP_pr32
SAD_pr02
AVLP_pr04
AVLP_pr12
AVLP/PVLP_pr01
AVLP_pr36
AVLP_pr05
IPS_pr01
AVLP_pr11
WED_pr02
IPS_pr02
AVLP_pr23
PVLP_pr03
SAD_pr01
AVLP_pr35
vpoEN
vpoIN
pMN1/DNp13
pMN2/vpoDN
pC2la
pC2lb
pC2lc
pC2ld
pC1d
pC1e
JO-A
JO-B
membrane contacts
25-128
membrane contacts
manually detected synapses (Kim et al., 2020)
0
100
200
300
400
500
600
700
300 nm
AVLP_pr01_R3
JON-A_R27
SAD_pr02_R8
JON-A_R38

Figure S4. Synaptic connections between each auditory cell type in FlyWire (both hemispheres) and membrane contacts between JONs and auditory neurons, related to Figure 5. A) Synaptic connections between each auditory cell type in FlyWire (both hemispheres). The number of synapses between every pair of neurons included in our EM connectivity analysis (see Figure 5; n=479 neurons), and organized by cell type. Synapse counts are based on an automated dataset[S1]. We include neurons from both the left and right hemisphere of the brain, and neurons with somas in the left hemisphere are listed first in each cell type grouping. Previously characterized auditory neurons are separated into their cell types according to[S2]. Synapses are plotted with presynaptic partners on the y-axis and postsynaptic partners on the x-axis. The color scale indicates the number of synapses between individual neuron pairs. B) Putative connections between JONs and auditory neurons. Number of membrane contact sites between 45 JON-A and 45 JON-B neurons[S3] and all auditory neurons. C) Total number of manually detected synapses[S3] vs. total number of membrane contacts between JONs and B1/GFN neurons. Best fit line equation is $y=0.84x+40$, $R^2=0.90$. D) Synapse from AVLP_pr01_R3 onto JON-A_R27. Inset shows 3D reconstructions of the same two neurons in FlyWire. Crosshairs indicate the corresponding position in the EM slice and inset (with red pointing medially and green pointing ventrally). E) Same as (D) for a synapse from SAD_pr02_R8 onto JON-A_R38. See also Table S3.

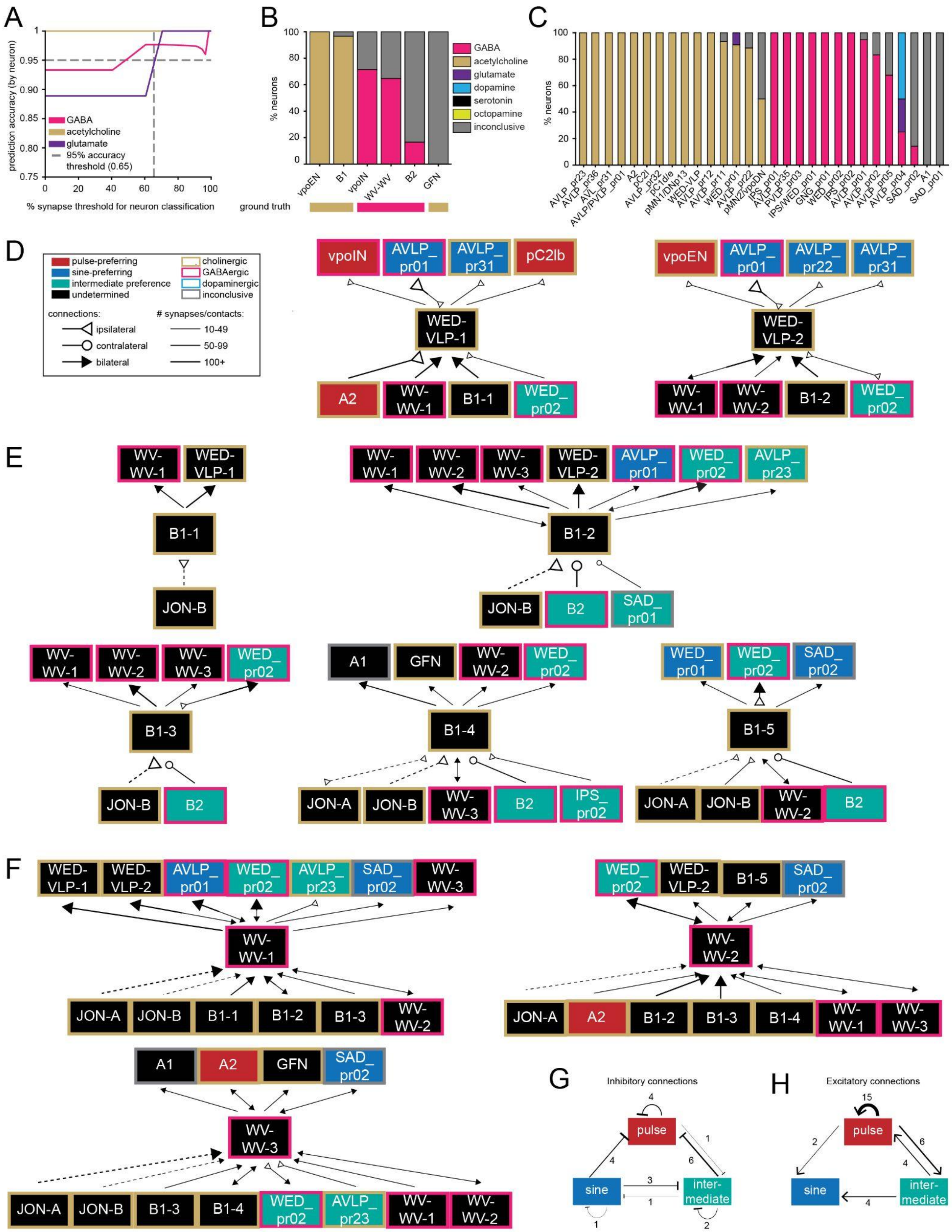

A
prediction accuracy (by neuron)
% synapse threshold for neuron classification
GABA
acetylcholine
glutamate
95% accuracy threshold (0.65)
B
% neurons
vpoEN
B1
vpoIN
WV-WV
B2
GFN
ground truth
GABA
acetylcholine
glutamate
dopamine
serotonin
octopamine
inconclusive
C
% neurons
D
pulse-preferring
sine-preferring
intermediate preference
undetermined
cholinergic
GABAergic
dopaminergic
inconclusive
connections:
ipsilateral
contralateral
bilateral
synapses/contacts:
10-49
50-99
100+
E
F
G
Inhibitory connections
H
Excitatory connections

Figure S5. Auditory connectome with previously identified auditory neurons divided into subtypes, related to Figure 5. A) Neurotransmitter prediction accuracy as a function of the fraction of synapses that have been predicted as the respective majority neurotransmitter. Data come from a test set of 135 neurons in a prior study[S4]. A threshold of 65% of consensus synaptic neurotransmitter predictions across a neuron's synapses results in greater than 95% classification accuracy for the three "classical" neurotransmitters. We used this threshold for predicting the neurotransmitters of auditory neurons. B) We compared neurotransmitter predictions for six cell types with their classifications from the literature based on fluorescence in-situ hybridization or antibody staining[S5–S8]. The deep learning-based classifier predictions for each neuron of a cell type (in the FAFB EM volume) are shown in the histogram, and the ground truth results from the literature are shown below. Neurons for which less than 65% of synapses are predicted to have the same neurotransmitter are labeled as "inconclusive" (grey). C) Classifier predictions for each cell type shown in Figure 5. The neurotransmitters used by these cell types have not been reported previously. D) Synaptic connectivity for cell types B1, WV-WV, WED-VLP broken down by their subtypes[S2,S8–S10]. The song mode preference of WED-VLP subtypes come from recordings of the split-GAL4 lines labeling neurons from the broader cell class. G) Number of inhibitory connections among all central auditory neurons (excluding JONs) based on pre- and postsynaptic preference classes. H) Same as (G) for excitatory connections. See also Table S3.

Abbreviation	**Neuropil**
AL	antennal lobe
AME	accessory medulla
AMMC	antennal mechanosensory and motor center
AOTU	anterior optic tubercle
ATL	antler
AVLP	anterior ventrolateral protocerebrum
BU	bulb
CAN	cantle
CRE	crepine
EB	ellipsoid body
EPA	epaulette
FB	fan-shaped body
FLA	flange
GA	gall
GNG	gnathal ganglion
GOR	gorget
IB	inferior bridge
ICL	inferior clamp
IPS	inferior posterior slope
LAL	lateral accessory lobe
LH	lateral horn
LO	lobula
LOP	lobula plate
MB-CA	mushroom body calyx
MB-ML	mushroom body medial lobe

MB-PED	mushroom body pedunculus
MB-VL	mushroom body vertical lobe
ME	medulla
NO	nodulus
PB	protocerebral bridge
PLP	posterior lateral protocerebrum
PRW	prow
PVLP	posterior ventrolateral protocerebrum
SAD	saddle
SCL	superior clamp
SIP	superior intermediate protocerebrum
SLP	superior lateral protocerebrum
SMP	superior medial protocerebrum
SPS	superior posterior slope
VES	vest
WED	wedge

Table S1. Neuropil abbreviations, related to Figures 1, S2, S3, and Table S2.

Split-GAL4 line ID	Existing name from literature or WED/VLP cell class name based on primary neuropil targeted
SS16374	AVLP_pr01
SS17963	AVLP_pr03
SS21914	AVLP_pr04
SS23281	AVLP_pr05 / AVLP-PN1 [S11]
SS23627	AVLP_pr06
SS27880	AVLP_pr07
SS27883	AVLP_pr08
SS27885	AVLP_pr02
SS27919	WED-VLP [S2] / IVLP-VLP [S7]
SS27932	IPS_pr01/ WED-PN1 [S11]
SS27936	WED_pr01
SS27953	AVLP_pr09
SS28822	AVLP_pr10
SS29136	AVLP_pr11
SS29146	AVLP_pr12
SS35318	AVLP_pr13
SS35456	AVLP_pr14
SS35471	AVLP_pr15
SS35473	A2 [S7]
SS35484	AVLP_pr16
SS35488	SLP_pr01
SS35489	AVLP_pr17
SS35502	AVLP_pr18
SS35504	PLP_pr01

SS35916	WED_pr02
SS35920	IC/SPS_pr01
SS35944	AVLP_pr19
SS35996	AVLP/PVLP_pr01
SS36007	GNG_pr01
SS36012	IPS_pr02
SS36521	PVLP_pr01
SS36541	AVLP_pr20
SS36960	AVLP_pr21
SS36971	SIP_pr01
SS36978	B1 [S7,S12] / aPN1 [S13]
SS37007	AVLP_pr22
SS38918	AVLP_pr23 / AV2 [S14]
SS38928	PVLP_pr02
SS38958	IPS_pr03
SS38981	B2 [S6,S12]
SS40303	IPS/WED_pr01
SS40316	PVLP_pr03
SS40354	AVLP_pr24
SS40361	AVLP_pr25
SS40366	AVLP_pr26
SS41342	AVLP_pr27
SS41376	AVLP_pr28
SS41378	AVLP_pr29
SS41685	AVLP_pr30
SS41704	PLP_pr02

SS41728	AVLP_pr31
SS41730	AVLP_pr32
SS41739	SAD_pr01
SS43299	SAD_pr02
SS43321	SAD/AMMC_pr01
SS43460	AVLP_pr33
SS43466	SMP_pr01
SS44510	IB_pr01
SS44818	AVLP_pr34
SS45858	AVLP_pr35
SS47261	AVLP_pr36
SS47509	AVLP_pr37
SS47517	WED_pr03
SS47537	PVLP_pr04
SS49115	AVLP_pr38

Table S2. Name of WED/VLP cell class in each split-GAL4 line, related to Figures 1-7, S1-2, 4-5.

Supplement References

S1. Buhmann, J., Sheridan, A., Malin-Mayor, C., Schlegel, P., Gerhard, S., Kazimiers, T., Krause, R., Nguyen, T.M., Heinrich, L., Lee, W.-C.A., *et al.* (2021). Automatic detection of synaptic partners in a whole-brain Drosophila electron microscopy data set. Nature Methods *18*, 771–774.

S2. Dorkenwald, S., McKellar, C.E., Macrina, T., Kemnitz, N., Lee, K., Lu, R., Wu, J., Popovych, S., Mitchell, E., Nehoran, B., *et al.* (2022). FlyWire: online community for whole-brain connectomics. Nat. Methods *19*, 119–128.

S3. Kim, H., Horigome, M., Ishikawa, Y., Li, F., Lauritzen, J.S., Card, G., Bock, D.D., and Kamikouchi, A. (2020). Wiring patterns from auditory sensory neurons to the escape and song-relay pathways in fruit flies. J. Comp. Neurol. *528*, 2068–2098.

S4. Eckstein, N., Bates, A.S., Du, M., Hartenstein, V., Gregory S X, and Funke, J. (2020). Neurotransmitter Classification from Electron Microscopy Images at Synaptic Sites in Drosophila. bioRxiv, 2020.06.12.148775.

S5. Allen, M.J., and Murphey, R.K. (2007). The chemical component of the mixed GF-TTMn synapse in Drosophila melanogaster uses acetylcholine as its neurotransmitter. Eur. J. Neurosci. *26*, 439–445.

S6. Tootoonian, S., Coen, P., Kawai, R., and Murthy, M. (2012). Neural representations of courtship song in the Drosophila brain. J. Neurosci. *32*, 787–798.

S7. Lai, J.S.-Y., Lo, S.-J., Dickson, B.J., and Chiang, A.-S. (2012). Auditory circuit in the Drosophila brain. Proc. Natl. Acad. Sci. U. S. A. *109*, 2607–2612.

S8. Wang, K, Wang, F, Forknall, N, Yang, T, Patrick, C, Parekh, R, Dickson, BJ (2021). Neural circuit mechanisms of sexual receptivity in Drosophila females. Nature. *589*, 577-581.

S9. Deutsch, D., Pacheco, D., Encarnacion-Rivera, L., Pereira, T., Fathy, R., Clemens, J., Girardin, C., Calhoun, A., Ireland, E., Burke, A., *et al.* (2020). The neural basis for a persistent internal state in Drosophila females. eLife *9*:e59502.

S10. Shan Xu, C., Januszewski, M., Lu, Z., Takemura, S.-Y., Hayworth, K.J., Huang, G., Shinomiya, K., Maitin-Shepard, J., Ackerman, D., Berg, S., *et al.* (2020). A Connectome of the Adult Drosophila Central Brain. bioRxiv, 2020.01.21.911859.

S11. Dolan, M.-J., Frechter, S., Bates, A.S., Dan, C., Huoviala, P., Roberts, R.J., Schlegel, P., Dhawan, S., Tabano, R., Dionne, H., *et al.* (2019). Neurogenetic dissection of the Drosophila lateral horn reveals major outputs, diverse behavioural functions, and interactions with the mushroom body. eLife *8*:e43079.

S12. Kamikouchi, A., Inagaki, H.K., Effertz, T., Hendrich, O., Fiala, A., Göpfert, M.C., and Ito, K. (2009). The neural basis of Drosophila gravity-sensing and hearing. Nature *458*, 165–171.

S13. Vaughan, A.G., Zhou, C., Manoli, D.S., and Baker, B.S. (2014). Neural pathways for the detection and discrimination of conspecific song in D. melanogaster. Curr. Biol. *24*, 1039–

1049.

S14. Clemens, J., Girardin, C.C., Coen, P., Guan, X.-J., Dickson, B.J., and Murthy, M. (2015). Connecting Neural Codes with Behavior in the Auditory System of Drosophila. Neuron *87*, 1332–1343.